Chapter 11
Modelling of Two-dimensional Timoshenko Beams in Hencky Fashion

Emilio Turco

Abstract We describe a novel mechanical model of planar Timoshenko beam for large displacements analysis in elastic regime following Hencky beam model guidelines. More precisely, we model the strain energy of the beam in a discrete form by considering, besides the bending contribution, both the stretching and the sliding contributions. In this way a discrete model of Timoshenko beam is generated. This model, besides to be interesting *di per sé* has strong applications in the study of metamaterials based on beam lattices where, sometimes, the approximations introduced by the use of Euler–Bernoulli beam model are too rough for capturing some desired details. In addition, this is an intermediate step toward the construction of discrete three-dimensional Timoshenko beam models.

Keywords: Two-dimensional Timoshenko beam · Large displacements in elastic regime · Buckling of beams

11.1 Introduction

The Timoshenko beam model is the object of several scientific studies of historical kind (see, e.g., Elishakoff, 2020), of mathematical kind (see, e.g., Della Corte et al, 2019), both for static (Balobanov and Niiranen, 2018; Kiendl et al, 2015; Turco et al, 2020) and dynamic problems (Luu et al, 2015; Cazzani et al, 2016b,c,a). All these studies prove the great interest about this model both *di per sé* and also from the point of view of the technical applications.This interest is increased in last years for the large use of this model in the analysis of metamaterials when their internal structure requires beam models richer than the so-called Euler–Bernoulli beam (see, e.g., Meza et al, 2017, 2014; Gross et al, 2019; Vangelatos et al, 2019a,b).

E. Turco
Department of Architecture, Design and Urban planning (DADU), University of Sassari, Italy
e-mail: emilio.turco@uniss.it

B. E. Abali and I. Giorgio (eds.), *Developments and Novel Approaches in Nonlinear Solid Body Mechanics*, Advanced Structured Materials 130,
https://doi.org/10.1007/978-3-030-50460-1_11

By considering, for instance, pantographic metamaterials as described in the recent papers (dell'Isola et al, 2019b,a), the beams forming the pantographic sheet might have dimensions which suggest to consider the shear deformability instead of neglecting it *a priori* choosing the Euler–Bernoulli model. The Timoshenko beam model is obviously more expensive than Euler–Bernoulli model since the former requires to describe the rotations which are independent from displacements. However, this extra computational cost could balance, at least partially, a richer – therefore more accurate in principle – model.

The discrete form used for modelling the Timoshenko beam which will be described in this work is largely inspired by the work of Hencky (1921), although here both the stretching and the sliding terms of the strain are considered. Starting from the guidelines reported in Eremeyev and Altenbach (2017); Turco (2018); Eremeyev (2019) for describing the bending strain for three-dimensional beams, here, limiting ourselves to two-dimensional beams, we introduce in a simple way the stretching and the sliding strain measures. Since the discrete model presented here uses, besides Lagrangian parameters for describing the rotation field, also the nodal displacements, it makes simpler the treatment of systems of beams when the kinematical constraints on the nodes have to be imposed, as is necessary for pantographic structures.

After this brief Introduction, it will be presented the discrete model of a two-dimensional Timoshenko beam in the framework of Hencky approach, Section 11.2, defining completely the strain energy and, therefore, both the structural reaction and the stiffness matrix which are the main tools used in a path-following strategy such as proposed by Riks (1972), Section 11.3. Some numerical results showing the influence of the shear deformability are presented and discussed in Sec. 11.4. Finally, some concluding remarks along with a list of forthcoming issues are presented in Section 11.5.

11.2 Modelling of Two-Dimensional Timoshenko Beams

We consider a planar rectilinear beam[1] discretized by means of a series of links of equal length ℓ (for the sake of simplicity) connected by joints, see Fig. 11.1 sketched as black circles.

The position of j-th joint in the reference and in the current configuration is P_j and p_j, respectively. In the spirit of Cosserat brothers for one-dimensional continuum and of the Timoshenko beam model, each joint is also equipped, in the reference configuration, with a unit vector D_j which is transformed in the current configuration in the unit vector $\mathbf{d}_j = \mathbf{Q}_j\mathbf{D}_j$ being $\mathbf{Q}_j$ a proper orthogonal tensor which represents a rotation. Reference and current configurations are described by the sets $\{P_j, \mathbf{D}_j\}$ and $\{p_j, \mathbf{d}_j\}$, respectively. We remark that using the immediately above hypotheses the Lagrangian parameters used for describing the motion is the displacement of

[1] The rectilinear hypothesis can easily be removed to represent broken lines approximating curves.

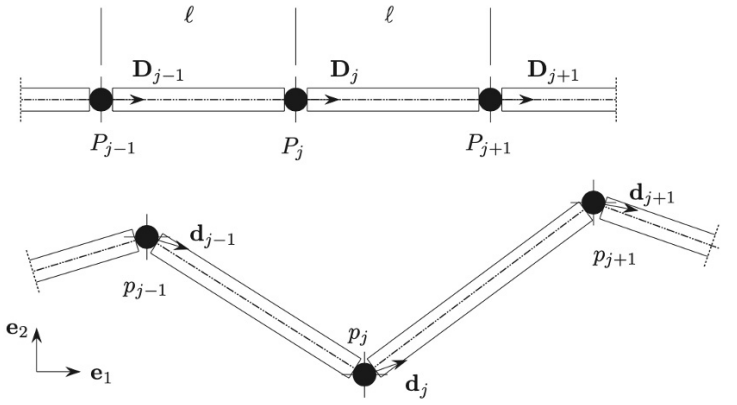

Fig. 11.1 Reference and current configuration of a segment of planar Timoshenko beam discretized à la Hencky.

j-th joint $\mathbf{w}_j = p_j - P_j$ and the rotation associated with the j-th proper orthogonal tensor $\mathbf{Q}_j$.

Looking again at Fig. 11.1, we can define as strain measures the vector $\Delta\mathbf{w}_{j+1}$

$$\Delta\mathbf{w}_{j+1} = (p_{j+1} - p_j) - \ell\mathbf{Q}_j\mathbf{D}_j\,, \tag{11.1}$$

and the tensor $\Delta\mathbf{P}_{j+1}$

$$\Delta\mathbf{P}_{j+1} = \mathbf{Q}_j^T\mathbf{Q}_{j+1}\,. \tag{11.2}$$

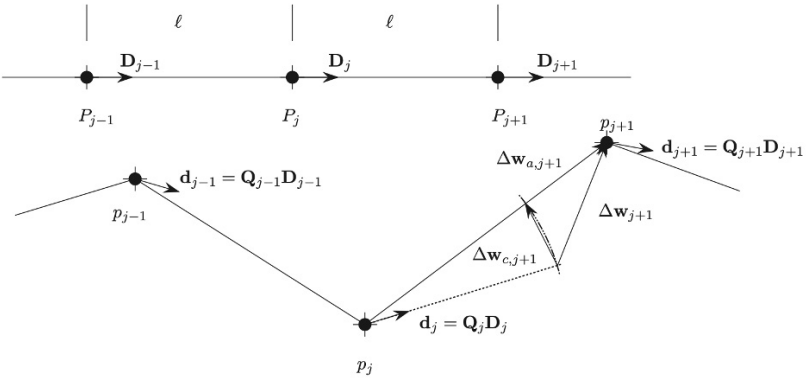

Fig. 11.2 Strain measures for a planar Timoshenko beam discretized à la Hencky.

The vector $\Delta\mathbf{w}_{j+1}$, i.e. the difference between $p_{j+1} - p_j$ (the vector which connects the j-th and $(j+1)$-th current positions) and $\ell\mathbf{Q}_j\mathbf{D}_j$ (that is the vector having ℓ norm obtained rotating $\mathbf{D}_j$ by $\mathbf{Q}_j$). The just defined strain vector $\Delta\mathbf{w}_{j+1}$, can be decomposed in two parts:

$$\Delta\mathbf{w}_{a,j+1} = (p_{j+i} - p_j)\left(1 - \frac{\ell}{\|p_{j+i} - p_j\|}\right), \tag{11.3}$$

$$\Delta\mathbf{w}_{c,j+1} = \Delta\mathbf{w}_{j+1} - \Delta\mathbf{w}_{a,j+1}\,, \tag{11.4}$$

being the graphic representation of each one sketched in Fig. 11.2.

The norms of these two vectors describe the stretching and the sliding, respectively, of the link in-between j and $j+1$ joints.

The proper orthogonal tensor $\Delta\mathbf{P}_{j+1}$ describes the bending that is the relative rotation between the two considered links. In details, as reported in Turco (2018) for the case of three-dimensional inextensible Euler–Benoulli beams, from Rodrigues' formula, see Rodrigues (1840), the relation between a rotation of amplitude φ about the rotation axis depicted by the unit vector $\mathbf{e}$ is represented by the proper orthogonal tensor $\mathbf{Q}$ expressed by[2]

$$\mathbf{Q} = \cos\varphi\mathbf{I} + (1 - \cos\varphi)\mathbf{e}\otimes\mathbf{e} + \sin\varphi\mathbf{E}\,, \tag{11.5}$$

being $\mathbf{I}$ and $\mathbf{E}$ the identity tensor and the skew tensor defined by the equivalence $\mathbf{E}\mathbf{u} = \mathbf{e}\times\mathbf{u}$, respectively.

Equation (11.5) define the rotation tensor as function of the rotation angle φ and the rotation axis $\mathbf{e}$. If we are interested to the rotation angle and to the rotation axis starting from the rotation tensor, taking into account that $\mathbf{E}$ is skew so $\mathrm{tr}(\mathbf{E}) = 0$ and $\mathbf{E}^T = -\mathbf{E}$, we can simply evaluate the trace of $\mathbf{Q}$:

$$\mathrm{tr}(\mathbf{Q}) = 2\cos\varphi + 1\,, \tag{11.6}$$

and the difference

$$\mathbf{Q} - \mathbf{Q}^T = 2\sin\varphi\mathbf{E}\,, \tag{11.7}$$

from which we can compute the vectorial invariant $\mathbf{Q}_\times$ of $\mathbf{Q}$, in formula:

$$\mathbf{Q}_\times = \sin\varphi\mathbf{e}\,. \tag{11.8}$$

From Eqs. (11.6) and (11.8) we have

$$\frac{\sin\varphi\mathbf{e}}{1+\cos\varphi} = \frac{2\mathbf{Q}_\times}{1+\mathrm{tr}(\mathbf{Q})}\,, \tag{11.9}$$

and finally, by using the bisection formula, we obtain

[2] It is better to treat the problem in 3D and successively simplify the results to the considered two-dimensional case, i.e. $\mathbf{e} = \mathbf{e}_3$.

$$2\tan\frac{\varphi}{2}\mathbf{e} = \frac{4\mathbf{Q}_\times}{1+\mathrm{tr}(\mathbf{Q})}\,. \tag{11.10}$$

Formula (11.10) suggest the use of variable $2\tan\frac{\varphi}{2}$, instead of φ, to describe the rotation angle. With this change of variable, Rodrigues formula can be written as

$$\mathbf{Q} = \frac{1}{4+\vartheta^2}\left((4-\vartheta^2)\mathbf{I} + 2\boldsymbol{\theta}\otimes\boldsymbol{\theta} + 4\vartheta\mathbf{E}\right)\,, \tag{11.11}$$

where $\boldsymbol{\theta} = \vartheta\mathbf{e}$ and $\vartheta^2 = \boldsymbol{\theta}\cdot\boldsymbol{\theta}$.

For two-dimensional Timoshenko beams, the kinematics is simpler since the rotation axis is always directed along the unit vector $\mathbf{e}_3$. For example, the skew tensor $\mathbf{E}$ and the rotation tensor $\mathbf{Q}$ become

$$\mathbf{E} = \begin{bmatrix} 0 & -1 & 0 \\ 1 & 0 & 0 \\ 0 & 0 & 0 \end{bmatrix}\,, \tag{11.12}$$

and

$$\mathbf{Q} = \begin{bmatrix} \cos\varphi & -\sin\varphi & 0 \\ \sin\varphi & \cos\varphi & 0 \\ 0 & 0 & 1 \end{bmatrix} \quad \text{or} \quad \mathbf{Q} = \frac{1}{4+\vartheta^2}\begin{bmatrix} 4-\vartheta^2 & -4\vartheta & 0 \\ 4\vartheta & 4-\vartheta^2 & 0 \\ 0 & 0 & 4+\vartheta^2 \end{bmatrix}\,, \tag{11.13}$$

respectively.

In the foregoing we have described the relationships between Lagrangian parameters used to describe the motion, i.e. the displacements of joints and the rotations of the links which, following the Timoshenko guidelines have to be independent, and the chosen strain measures $\Delta\mathbf{w}_{a,j}$, $\Delta\mathbf{w}_{c,j}$ and $\Delta\mathbf{P}_{j+1}$. Correspondingly, we can write the strain energy of the beam just summing the following elementary contributions:

$$2E_a = a\|\Delta\mathbf{w}_{a,j+1}\|^2\,, \tag{11.14}$$

$$2E_b = b\|\Delta\boldsymbol{\phi}_{j+1}\|^2\,, \tag{11.15}$$

$$2E_c = c\|\Delta\mathbf{w}_{c,j+1}\|^2\,, \tag{11.16}$$

where, besides the quantities already defined, we use $\Delta\boldsymbol{\phi}_{j+1}$ which is the finite relative rotation vector associated to $\Delta\mathbf{P}_{j+1}$ by using the link defined by Eq. (11.10) and a, b and c are the stiffness parameters related to stretching, bending and sliding. We remark that in the considered case $\Delta\boldsymbol{\phi}_{j+1}$ has only one component different from zero, i.e. the third.

Finally we observe that in the case of $\mathbf{d}_j$ directed as the segment in-between j and $j+1$ there is not sliding and we come back to the Hencky approximation of the Euler–Bernoulli model as described, e.g., in Turco et al (2016).

11.3 Numerically Driven Drawing of the Equilibrium Path

Enforcing the stationarity condition for the potential energy with respect to nodal displacements vector $\mathbf{u}$, the nonlinear system of equilibrium equations can be written as

$$\mathbf{s}[\mathbf{u}] - \mathbf{p}[\lambda] = \mathbf{0}\,, \tag{11.17}$$

being the vector $\mathbf{s}$ the structural reaction, depending upon nodal displacement vector $\mathbf{u}$, and $\mathbf{p}[\lambda]$ the external load vector ruled by the dimensionless load parameter λ. The structural reaction $\mathbf{s}$ can be computed starting from the total strain energy E of the system, i.e. adding the contributions deriving from (11.14), (11.15) and (11.16), as

$$\mathbf{s} = \frac{dE}{d\mathbf{u}}\,, \tag{11.18}$$

while, the external load is expressed in the form

$$\mathbf{p}[\lambda] = \mathbf{p}_0 + \lambda\widehat{\mathbf{p}}\,, \tag{11.19}$$

able to represent both external loads $\lambda\widehat{\mathbf{p}}$ which increase with the dimensionless parameter λ and external loads independent from λ, i.e. $\mathbf{p}_0$. This load representation is useful to model the so-called load imperfections.

The solution of the nonlinear system of equations (11.17) could be obtained by using a stepwise procedure which uses the Newton's method. Starting from the pair $(\mathbf{u}_i, \lambda_i)$ which represents the i-th equilibrium point, the next one, and nearby, $(\mathbf{u}_i + \Delta\mathbf{u}, \lambda_i + \Delta\lambda)$ can be computed, by linearizing Eq. (11.17)

$$\mathbf{s}[\mathbf{u}_i] + \mathbf{K}\Delta\mathbf{u} - (\mathbf{p}_0 + (\lambda_i + \Delta\lambda)\widehat{\mathbf{p}}) \approx \mathbf{0}\,, \tag{11.20}$$

which uses the stiffness matrix $\mathbf{K}$ defined as

$$\mathbf{K} = \frac{d\mathbf{s}}{d\mathbf{u}}\,, \tag{11.21}$$

computed in $\mathbf{u}_i$. Newton's method, starting from the linearization (11.20), gives the recurrent formula to compute $\Delta\mathbf{u}$ when the value of $\Delta\lambda$ is fixed in advance:

$$\Delta\mathbf{u} = -\Delta\lambda\mathbf{K}^{-1}\widehat{\mathbf{p}}\,. \tag{11.22}$$

As is well documented in technical literature, Newton's method does not converge when $\mathbf{K}$ is singular or nearly-singular. In order to bypass this limitation, Riks Riks (1972) proposed the parametrization of the equilibrium path by means its arc-length instead of the dimensionless load parameter λ. The consequent integration scheme is not affected by the convergence problems intrinsic in the Newton's method, but it has to be completed by an additional equation.

In some detail, Riks' arc-length scheme proposes a correction on the extrapolation obtained from Newton formula (11.22). If the pair $(\mathbf{u}_i, \lambda_i)$ is an equilibrium point and $(\Delta\mathbf{u}, \Delta\lambda)$ is a Newton extrapolation, the Riks correction $(\dot{\mathbf{u}}, \dot{\lambda})$ can be evaluated

from the linearization (11.17) in the point $(\mathbf{u}_i + \Delta\mathbf{u}, \lambda_i + \Delta\lambda)$

$$\mathbf{s}\,[\mathbf{u}_i + \Delta\mathbf{u}] + \mathbf{K}\dot{\mathbf{u}} - (\mathbf{p}_0 + (\lambda_i + \Delta\lambda + \dot{\lambda})\widehat{\mathbf{p}}) \approx \mathbf{0}\,, \tag{11.23}$$

where the stiffness matrix $\mathbf{K}$ is now computed in $\mathbf{u}_i + \Delta\mathbf{u}$. From (11.23) $\dot{\mathbf{u}}$ can be computed from

$$\dot{\mathbf{u}} = -\mathbf{K}^{-1}\left(\mathbf{s}[\mathbf{u}_i + \Delta\mathbf{u}] - (\mathbf{p}_0 + (\lambda_i + \Delta\lambda + \dot{\lambda})\widehat{\mathbf{p}})\right)\,, \tag{11.24}$$

The additional equation required to compensate the unknown $\dot{\lambda}$ can be chosen in several different ways. One producing a very simple formula, also computationally convenient, is

$$\Delta\mathbf{u} \cdot \mathbf{K}\dot{\mathbf{u}} = 0\,, \tag{11.25}$$

which enforces the $\mathbf{K}$-orthogonality between the Newton extrapolation $\Delta\mathbf{u}$ and the Riks correction $\dot{\mathbf{u}}$. Substituting (11.24) in (11.25) and taking also into account (11.22), simple calculations give the straightforward expression

$$\dot{\lambda} = \frac{\widehat{\mathbf{u}} \cdot \mathbf{r}}{\widehat{\mathbf{u}} \cdot \widehat{\mathbf{p}}}\,, \tag{11.26}$$

being $\mathbf{r} = \mathbf{s}[\mathbf{u}_i + \Delta\mathbf{u}] - (\mathbf{p}_0 + (\lambda_i + \Delta\lambda)\widehat{\mathbf{p}})$ the rest of equilibrium equations and $\widehat{\mathbf{u}} = \mathbf{K}^{-1}\widehat{\mathbf{p}}$ (from (11.22)). Finally, from (11.24), the Riks correction $\dot{\mathbf{u}}$ can be computed making use of Newton extrapolation $\Delta\mathbf{u}$.

Formulae (11.26), (11.24) and (11.22) fully define the Riks-based algorithm once the first extrapolation is defined:

$$\Delta\lambda = \mu(\lambda_i - \lambda_{i-1})\,, \tag{11.27}$$

$$\Delta\mathbf{u} = \mu(\mathbf{u}_i - \mathbf{u}_{i-1})\,, \tag{11.28}$$

here, μ is an adaptive coefficient used to vary the arc-length during the stepwise procedure and the pairs $(\lambda_i, \mathbf{u}_i)$ and $(\lambda_{i-1}, \mathbf{u}_{i-1})$ the last and the second last computed point of the equilibrium path, respectively. Synthetically, the adaptive coefficient μ drives the step-length of each step on the nonlinearity of the equilibrium path. A straightforward expression for computing μ, is suggested in Wriggers (2008); Clarke and Hancock (1990):

$$\mu = 1 - \frac{r_l - n_l}{r_l + n_l}\,, \tag{11.29}$$

it uses the number of required loops r_l to reach the convergence in the current step and the number of needed loops n_l (the usual choiche is $n_l = 5$). At the beginning of the analysis process $\mu = 1$ is assumed, whereas the value of $\Delta\lambda$ is estimated by some auxiliary analysis. The initial settings of $\Delta\lambda$ and of $\Delta\mathbf{u}$ fix, implicitly, the curve arc-length.

11.4 Quantitative Analysis of the Influence of the Shear Stiffness Parameter

The quantitative difference between the discrete form of the Euler–Bernoulli and Timoshenko beam models can be estimated in a simple way by referring to a cantilever beam ℓ long loaded with a transversal force F on the free end. If we compute, in the case of linear elasticity and for small displacements, the transversal displacement of the free end, neglecting the deformation due to the shear, we have $F\ell^3/3EI$ being E and I the Young modulus of the material and the inertia of the cross-section, respectively. Therefore, the bending stiffness is $3EI/\ell^3$. Conversely, the contribution related to the shear deformability is $F\ell/GA^*$ being G and A^* the shear modulus of the material and the reduced area of the cross-section, respectively. The corresponding shear stiffness is GA^*/ℓ. If we compute the ratio between the displacement of the free end due to the shear and to the bending contributions we have

$$\frac{w_s}{w_b} = \frac{\dfrac{3EI}{\ell^3}}{\dfrac{GA^*}{\ell}}, \tag{11.30}$$

from which we deduce that this ratio is inversely proportional to the square of the beam length. If we consider a beam with rectangular cross-section b depth and h height, the ratio becomes

$$\frac{w_s}{w_b} \propto \left(\frac{h}{\ell}\right)^2, \tag{11.31}$$

besides to be dependent from the Poisson's ratio. For example, for $h/\ell = 0.5$ the shear term is equal to the 25% of bending term and so surely not negligible.

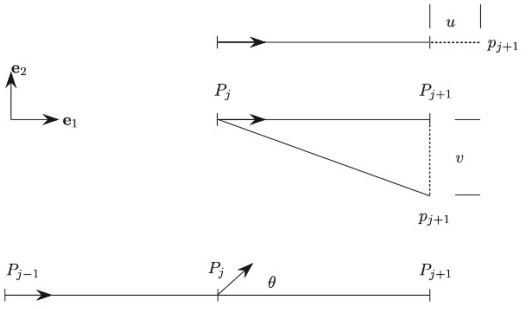

Fig. 11.3 Deformation modes: stretching (on the top), sliding (on the middle) and bending (on the bottom).

Starting from this simple analysis, we can compute numerically the values of the energy related to stretching, bending and sliding following Eqs. (11.14), (11.15) and (11.16). Therefore, for large displacements, we consider the three representative deformation modes sketched in Fig. 11.3:

1. the first one considers the points P_j and P_{j+1} and the deformation corresponding to $p_{j+1} = P_{j+1} + u\mathbf{e}_1$ keeping $p_j = P_j$;
2. the second one, always for the points P_j and P_{j+1}, considers the deformation corresponding to $p_{j+1} = P_{j+1} + v\mathbf{e}_2$ keeping $p_j = P_j$;
3. the third one considers for the links in-between three consecutive points P_{j-1}, P_j and P_{j+1} the rotations θ_j keeping $\theta_{j-1} = 0$.

Figure 11.4 reports the dimensionless strain energy split in stretching, bending and sliding contributions as function of the parameters u, v and θ_j. We remark that the parameter u influences only the stretching energy, v stretching and sliding and, finally, θ_j stretching, bending and sliding. Figure 11.5 reports the sliding-stretching strain energy ratio *versus* the dimensionless displacement v_j/ℓ varying the c/a ratio from 0.1 to 10 keeping unchanged b. Figure 11.6 shows as the sliding-bending strain energy ratio varies when the non-dimensional stiffness ratio $c\ell^2/b$ increases from 0.1 to 10 keeping unchanged a.

The last two plots show, also quantitatively, the influence of the sliding part of the energy, respect to the stretching and the bending part, when the stiffness parameter c increases. In addition, we notice that the sliding part of the strain energy decreases when the displacement parameter of the considered deformation mode increases.

11.4.1 Tip Deflection of a Cantilever Beam

By referring to the cantilever beam reported in Fig. 11.7 loaded with a transversal force on the tip, Figure 11.8 shows as the cantilever beam tip displacement varies when the load parameter λ increases varying the stiffness ratio c/b. As can be noticed from the plots, for large displacements the influence of the parameter c is relevant and surely it can not be neglected.

Figure 11.9 reports two deformations corresponding to the end of the loading path. They correspond to the values $c/b = 0.005$, on the left, and $c/b = 5$, on the right, respectively. Colors red and blue distinguish the current positions of nodes and of rotations, respectively. It can be noticed that the two deformations are very different. In the first one, see Fig. 11.9(a), the effect of sliding is clearly visible and it is described by the blue segments sharply distinct from the red line which describes the displacements. In the second one, see Fig. 11.9(b), blue segments and red line are overlapped showing that for the used c/b ratio the sliding is practically negligible and the Euler–Bernoulli beam model could be profitably used.

Figure 11.10 shows the strain energy evolution, when λ increases, for two limit cases, $c/b = 0.005$ on the left and $c/b = 5$ on the right. Small values of the sliding stiffness c, respect to bending stiffness b, give non-negligible values of the sliding strain energy, respect to the bending strain energy, whereas for higher values of c the relative contribution E_c is negligible, respect to the bending strain energy.

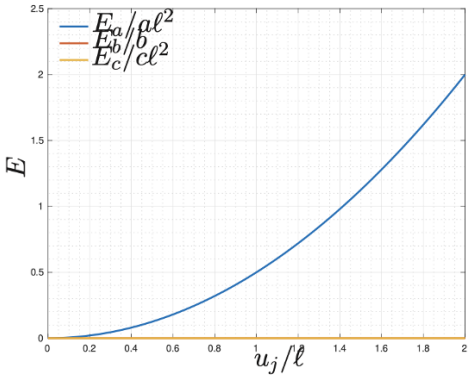

(a) Stretching deformation mode

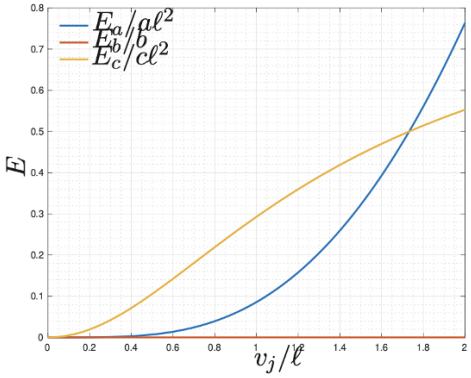

(b) Sliding deformation mode

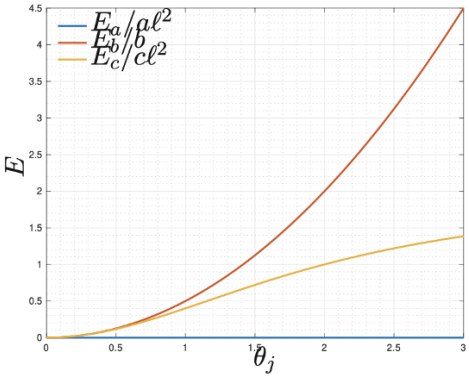

(c) Bending deformation mode

Fig. 11.4 Dimensionless strain energy, split in stretching, bending and sliding contributions, corresponding to deformation modes associated to u_j/ℓ, v_j/ℓ and θ_j.

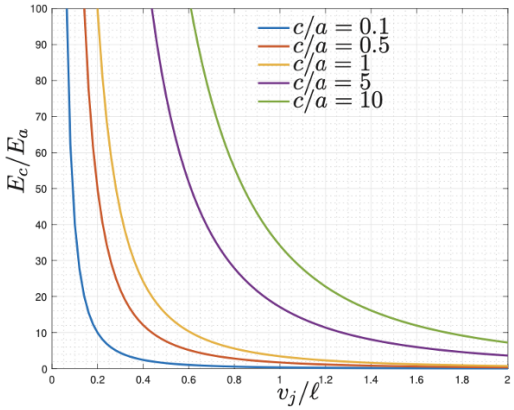

Fig. 11.5 Sliding-stretching strain energy ratio corresponding to the deformation modes associated to v_j/ℓ varying the c/a ratio from 0.1 to 10.

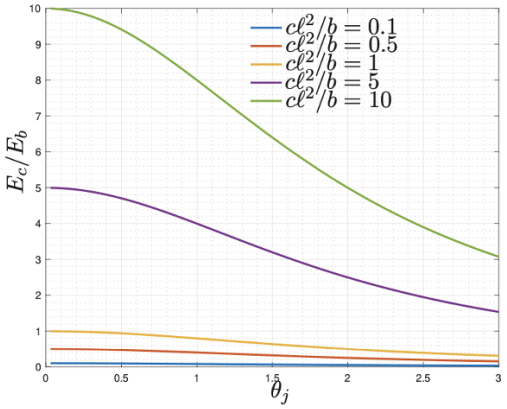

Fig. 11.6 Sliding-bending strain energy ratio corresponding to the deformation modes associated to θ_j varying the $c\ell^2/b$ ratio.

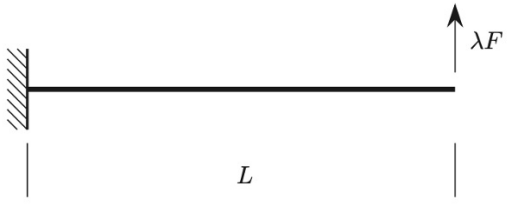

Fig. 11.7 Cantilever beam under a shear force on the tip.

11.4.2 Buckling of a Simply Supported Beam

By referring to the simply-supported beam depicted in Fig. 11.11 loaded with a compression force ruled by the load parameter λ and a transversal force on the beam midpoint mimicking an imperfection load, Figure 11.12 shows as the dimensionless transversal displacement t/L of the midpoint varies when the load parameter λ

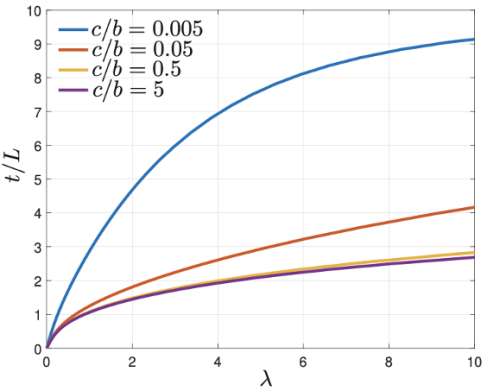

Fig. 11.8 Dimensionless cantilever beam tip displacement t/L loaded by a transversal force on the tip (L is the length of the beam) vs. the load parameter λ varying c/b ratio.

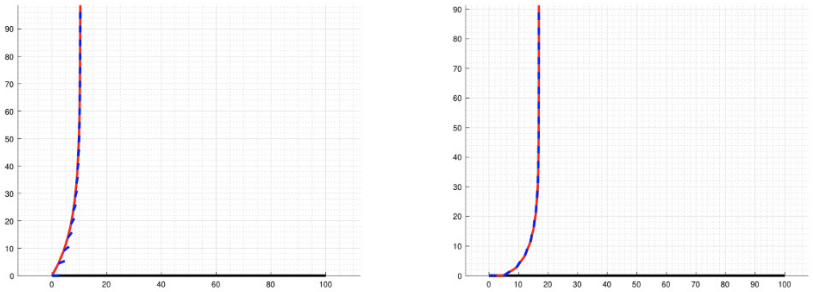

(a) $c/b = 0.005$ (b) $c/b = 5$

Fig. 11.9 Deformation for $c/ = 0.005$, on the left, and $c/b = 5$, on the right, (red color is used for current positions of nodes blue color for rotations.

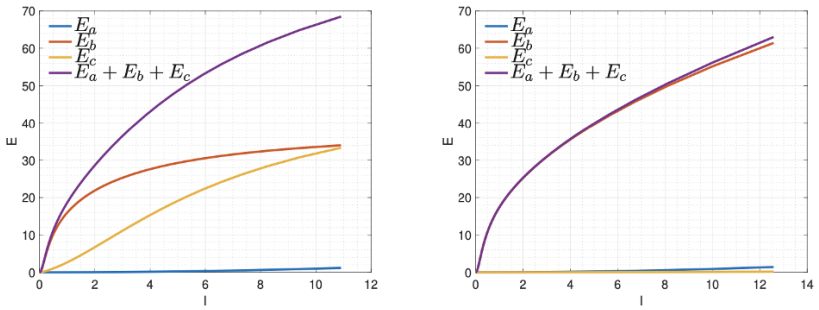

(a) $c/b = 0.005$ (b) $c/b = 5$

Fig. 11.10 Strain energy (total and split in stretching E_a, bending E_b and sliding E_c parts) for $c/b = 0.005$ (on the left) and $c/b = 5$ (on the right).

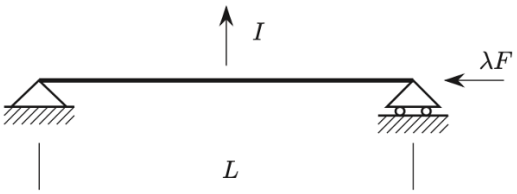

Fig. 11.11 Simply supported beam under compression load and transversal imperfection.

increases varying the stiffness ratio c/b. From the plots, we can guess, at least approximatively, the strong influence of c/b ratio on the buckling loads and on the first part of the secondary branches while last parts of the equilibrium paths are practically indistinguishable.

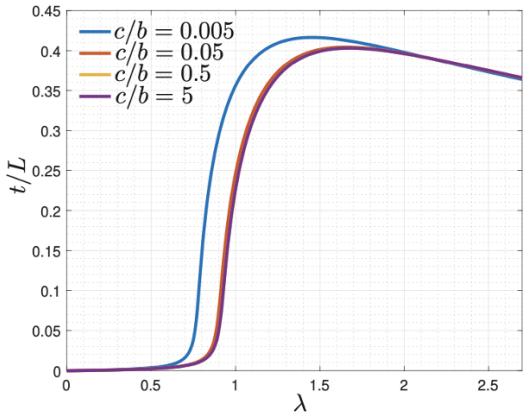

Fig. 11.12 Buckling of a simply supported beam: dimensionless midpoint displacement t/L (L is the length of the beam) vs. load parameter λ varying c/b ratio.

Figure 11.13 reports two deformations corresponding to the end of the loading path.[3] They correspond to the values $c/b = 0.005$, on the left, and $c/b = 5$, on the right, respectively. As in the foregoing, red and blue colors distinguish current positions of nodes and rotations, respectively. It can be noticed that the two deformations are very different. In the first one, see Fig. 11.13(a), the sliding effect, described by the blue segments sharply distinct from the red line which describes the displacements, is clearly visible. In the second one, see Fig. 11.13(b), blue segments and red line are overlapped showing that the used c/b ratio the sliding is practically negligible and the Euler–Bernoulli beam model could be profitably used.

Figure 11.14 shows the strain energy evolution, when λ increases, for two limit cases, $c/b = 0.005$ on the left and $c/b = 5$ on the right. Small values of the sliding stiffness c, respect to bending stiffness b, give non-negligible values of the sliding

[3] The Author is aware that these solutions are admissible only if the overlapping of the beam is allowed.

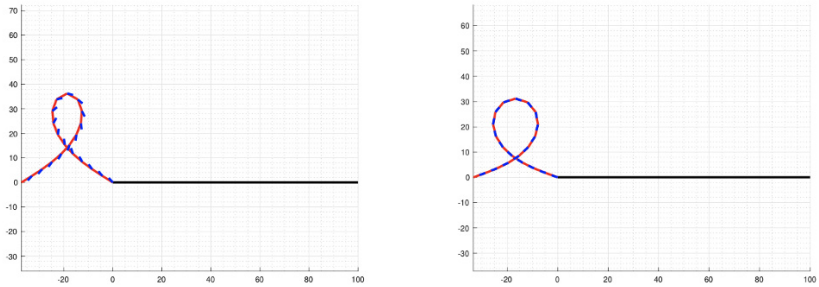

Fig. 11.13 Buckling of a simply supported beam: deformation for $c/b = 0.005$, on the left, and $c/b = 5$, on the right, (red color is used for current positions of nodes whereas in blue color for rotations.

strain energy, respect to the bending strain energy, whereas for higher values of c the relative contribution E_c is negligible, respect to the bending strain energy.

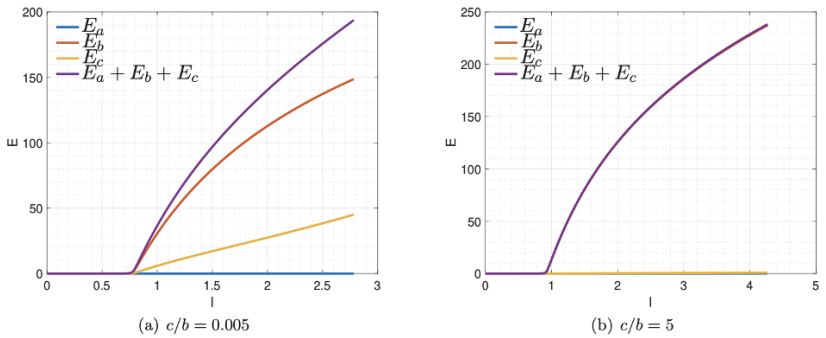

Fig. 11.14 Buckling of a simply supported beam: strain energy (total and split in stretching E_a, bending E_b and sliding E_c parts) for $c/b = 0.005$ (on the left) and $c/b = 5$ (on the right).

11.5 Concluding Remarks and Future Challenges

This work has presented and discussed a novel discrete mechanical model, largely inspired by the Hencky work, devoted to study two-dimensional Timoshenko beam. After the model presentation and a brief sketch of the algorithm used for reconstructing the equilibrium path, the results of some numerical simulations are used for evaluating the sensitivity of results respect to the shear stiffness parameter. In some detail, numerical simulations have shown that neglecting the shear deformation

can produce results almost far from those produced taking into account the shear contribution. This result is confirmed also when buckling problems for simple beams are considered.

After this preliminary work, there are several open problems to tackle, in particular: *i)* it is necessary a further careful analysis on the stiffness parameters used to model the elastic response of the discrete beam; these parameters should be linked to the usual constitutive parameters of the material, for instance the Young and the tangential stiffness moduli, and to the geometric parameters of the beam, for instance the transversal cross-section area, the inertia and the shear correction factor; in addition, the stiffness parameters of the discrete beam might be considered as variables along the beam (functionally graded materials); an extended campaign of numerical simulations might be discover new and exotic mechanical behaviors (see, e.g., Alibert et al, 2003; Seppecher et al, 2011; Misra et al, 2018; De Angelo et al, 2019; Turco et al, 2019; Scerrato and Giorgio, 2019); *ii)* it is intriguing the development of continuum models[4], such as reported, e.g., in Boutin et al (2017); Giorgio et al (2018, 2019); Barchiesi et al (2019b); Placidi et al (2020); Barchiesi et al (2019a); Abdoul-Anziz and Seppecher (2018); Abdoul-Anziz et al (2019); Andreaus et al (2018); Abali et al (2015); Spagnuolo and Andreaus (2019) based on the discrete model and on the results presented here; their use could help to identify the stiffness parameter of the discrete model besides to be useful for developing continuum models devoted to the analysis of plane or curved structures moulded as, e.g., shells and tubes (see Greco et al, 2018, 2019a,b; Greco and Cuomo, 2015; Greco, 2020; Abali et al, 2016; Yang et al, 2018); *iii)* it is promising the extension of elastic stability theory for micromorphic, strain-gradient media and granular materials, likewise the nonlinear elasticity theory (see, e.g. Ogden, 1997; Fu and Ogden, 1999), and to Cosserat media (see, e.g., Eremeev and Zubov, 1994; Sheydakov and Altenbach, 2016; Lakes, 2018; Solyaev et al, 2020; Balobanov and Niiranen, 2018; Misra and Poorsolhjouy, 2015; Pideri and Seppecher, 1997; dell'Isola et al, 2015; Niiranen et al, 2019); *iv)* it should be considered the extension to problems where dynamics effects have to necessarily be considered (see, e.g., Giorgio, 2020; Giorgio and Del Vescovo, 2019, 2018; Giorgio et al, 2017; Laudato and Barchiesi, 2019) or technical problems which consider the active control of vibrations (see Chróścielewski et al, 2019) and therein references.

Acknowledgements For this work I am indebted to many people of the M&MOCS International Research Center. I wish to thank all of them for their invaluable suggestions and fruitful discussions.

References

Abali BE, Müller WH, Eremeyev VA (2015) Strain gradient elasticity with geometric nonlinearities and its computational evaluation. Mechanics of Advanced Materials and Modern Processes

[4] See the exegesis of the work *Fundamentals of the mechanics of continua* by E. Hellinger reported in Eugster and dell'Isola (2017, 2018a,b) for an insightful analysis on the continuum idea.

1(1):1–11
Abali BE, Wu CC, Müller WH (2016) An energy-based method to determine material constants in nonlinear rheology with applications. Continuum Mechanics and Thermodynamics 28(5):1221–1246
Abdoul-Anziz H, Seppecher P (2018) Strain gradient and generalized continua obtained by homogenizing frame lattices. Mathematics and mechanics of complex systems 6(3):213–250
Abdoul-Anziz H, Seppecher P, Bellis C (2019) Homogenization of frame lattices leading to second gradient models coupling classical strain and strain-gradient terms. Mathematics and Mechanics of Solids 24(12):3976–3999
Alibert JJ, Seppecher P, dell'Isola F (2003) Truss modular beams with deformation energy depending on higher displacement gradients. Mathematics and Mechanics of Solids 8(1):51–73
Andreaus U, Spagnuolo M, Lekszycki T, Eugster SR (2018) A Ritz approach for the static analysis of planar pantographic structures modeled with nonlinear Euler–Bernoulli beams. Continuum Mechanics and Thermodynamics 30(5):1103–1123
Balobanov V, Niiranen J (2018) Locking-free variational formulations and isogeometric analysis for the Timoshenko beam models of strain gradient and classical elasticity. Computer Methods in Applied Mechanics and Engineering 339:137–159
Barchiesi E, Eugster SR, Placidi L, dell'Isola F (2019a) Pantographic beam: a complete second gradient 1d-continuum in plane. Zeitschrift für angewandte Mathematik und Physik 70(5):135
Barchiesi E, Ganzosch G, Liebold C, Placidi L, Grygoruk R, Müller WH (2019b) Out-of-plane buckling of pantographic fabrics in displacement-controlled shear tests: experimental results and model validation. Continuum Mechanics and Thermodynamics 31(1):33–45
Boutin C, dell'Isola F, Giorgio I, Placidi L (2017) Linear pantographic sheets: asymptotic micro-macro models identification. Mathematics and Mechanics of Complex Systems 5(2):127–162
Cazzani A, Stochino F, Turco E (2016a) An analytical assessment of finite element and isogeometric analyses of the whole spectrum of Timoshenko beams. ZAMM-Zeitschrift für Angewandte Mathematik und Mechanik 96(10):1220–1244
Cazzani A, Stochino F, Turco E (2016b) On the whole spectrum of Timoshenko beams. Part I: a theoretical revisitation. Zeitschrift für angewandte Mathematik und Physik 67(2):24
Cazzani A, Stochino F, Turco E (2016c) On the whole spectrum of Timoshenko beams. Part II: further applications. Zeitschrift für angewandte Mathematik und Physik 67(2):25
Chróścielewski J, Schmidt R, Eremeyev VA (2019) Nonlinear finite element modeling of vibration control of plane rod-type structural members with integrated piezoelectric patches. Continuum Mechanics and Thermodynamics 31(1):147–188
Clarke MJ, Hancock GJ (1990) A study of incremental-iterative strategies for non-linear analyses. International Journal for Numerical Methods in Engineering 29(7):1365–1391
De Angelo M, Barchiesi E, Giorgio I, Abali BE (2019) Numerical identification of constitutive parameters in reduced-order bi-dimensional models for pantographic structures: application to out-of-plane buckling. Archive of Applied Mechanics 89(7):1333–1358
Della Corte A, Battista A, dell'Isola F, Seppecher P (2019) Large deformations of Timoshenko and Euler beams under distributed load. Zeitschrift für angewandte Mathematik und Physik 70(2):52
dell'Isola F, Andreaus U, Placidi L (2015) At the origins and in the vanguard of peridynamics, non-local and higher-gradient continuum mechanics: an underestimated and still topical contribution of Gabrio Piola. Mathematics and Mechanics of Solids 20(8):887–928
dell'Isola F, Seppecher P, Alibert JJ, et al (2019a) Pantographic metamaterials: an example of mathematically driven design and of its technological challenges. Continuum Mechanics and Thermodynamics 31(4):851–884
dell'Isola F, Seppecher P, Spagnuolo M, et al (2019b) Advances in pantographic structures: design, manufacturing, models, experiments and image analyses. Continuum Mechanics and Thermodynamics 31(4):1231–1282
Elishakoff I (2020) Who developed the so-called Timoshenko beam theory? Mathematics and Mechanics of Solids 25(1):97–116

Eremeev VA, Zubov LM (1994) On the stability of elastic of elastic bodies with couple stresses. Mechanics of Solids 29(3):172–181

Eremeyev V, Altenbach H (2017) Basics of mechanics of micropolar shells. In: Shell-like Structures, vol 572, Springer, pp 63–111

Eremeyev VA (2019) Two-and three-dimensional elastic networks with rigid junctions: modeling within the theory of micropolar shells and solids. Acta Mechanica 230(11):3875–3887

Eugster SR, dell'Isola F (2017) Exegesis of the introduction and Sect. I from "Fundamentals of the mechanics of continua"** by E. Hellinger. ZAMM-Zeitschrift für Angewandte Mathematik und Mechanik 97(4):477–506

Eugster SR, dell'Isola F (2018a) Exegesis of Sect. II and III. A from "Fundamentals of the mechanics of continua" by E. Hellinger. ZAMM-Zeitschrift für Angewandte Mathematik und Mechanik 98(1):31–68

Eugster SR, dell'Isola F (2018b) Exegesis of Sect. III. B from "Fundamentals of the mechanics of continua" by E. Hellinger. ZAMM-Zeitschrift für Angewandte Mathematik und Mechanik 98(1):69–105

Fu YB, Ogden RW (1999) Nonlinear stability analysis of pre-stressed elastic bodies. Continuum Mechanics and Thermodynamics 11(3):141–172

Giorgio I (2020) A discrete formulation of Kirchhoff rods in large-motion dynamics. Mathematics and Mechanics of Solids 25(5):1081–1100

Giorgio I, Del Vescovo D (2018) Non-linear lumped-parameter modeling of planar multi-link manipulators with highly flexible arms. Robotics 7(4):60

Giorgio I, Del Vescovo D (2019) Energy-based trajectory tracking and vibration control for multilink highly flexible manipulators. Mathematics and Mechanics of Complex Systems 7(2):159–174

Giorgio I, Della Corte A, dell'Isola F (2017) Dynamics of 1D nonlinear pantographic continua. Nonlinear Dynamics 88(1):21–31

Giorgio I, dell'Isola F, Steigmann DJ (2018) Axisymmetric deformations of a 2nd grade elastic cylinder. Mechanics Research Communications 94:45–48

Giorgio I, dell'Isola F, Steigmann DJ (2019) Edge effects in hypar nets. Comptes Rendus Mécanique 347(2):114–123

Greco L (2020) An iso-parametric G^1-conforming finite element for the nonlinear analysis of Kirchhoff rod. Part I: the 2D case. Continuum Mechanics and Thermodynamics pp 1–24

Greco L, Cuomo M (2015) Consistent tangent operator for an exact Kirchhoff rod model. Continuum Mechanics and Thermodynamics 27(4-5):861–877

Greco L, Cuomo M, Contrafatto L (2018) A reconstructed local B formulation for isogeometric Kirchhoff–Love shells. Computer method in applied mechanics and engineering 332:462–487

Greco L, Cuomo M, Contrafatto L (2019a) A quadrilateral G1-conforming finite element for the Kirchhoff plate model. Computer Methods in Applied Mechanics and Engineering 346:913–951

Greco L, Cuomo M, Contrafatto L (2019b) Two new triangular G1-conforming finite elements with cubic edge rotation for the analysis of Kirchhoff plates. Computer Methods in Applied Mechanics and Engineering 356:354–386

Gross A, Pantidis P, Bertoldi K, Gerasimidis S (2019) Correlation between topology and elastic properties of imperfect truss-lattice materials. Journal of the Mechanics and Physics of Solids 124:577–598

Hencky H (1921) Über die angenäherte lösung von stabilitätsproblemen im raum mittels der elastischen gelenkkette. PhD thesis, Engelmann

Kiendl J, Auricchio F, Hughes TJ, Reali A (2015) Single-variable formulations and isogeometric discretizations for shear deformable beams. Computer Methods in Applied Mechanics and Engineering 284:988–1004

Lakes RS (2018) Stability of Cosserat solids: size effects, ellipticity and waves. Journal of Mechanics of Materials and Structures 13(1):83–91

Laudato M, Barchiesi E (2019) Non-linear dynamics of pantographic fabrics: modelling and numerical study. In: Wave Dynamics, Mechanics and Physics of Microstructured Metamaterials, Springer, pp 241–254

Luu AT, Kim NI, Lee J (2015) Isogeometric vibration analysis of free-form Timoshenko curved beams. Meccanica 50(1):169–187

Meza LR, Das S, Greer JR (2014) Strong, lightweight, and recoverable three-dimensional ceramic nanolattices. Science 345(6202):1322–1326

Meza LR, Phlipot GP, Portela CM, et al (2017) Reexamining the mechanical property space of three-dimensional lattice architectures. Acta Materialia 140:424–432

Misra A, Poorsolhjouy P (2015) Identification of higher-order elastic constants for grain assemblies based upon granular micromechanics. Mathematics and Mechanics of Complex Systems 3(3):285–308

Misra A, Lekszycki T, Giorgio I, Ganzosch G, Müller WH, dell'Isola F (2018) Pantographic metamaterials show atypical poynting effect reversal. Mechanics Research Communications 89:6–10

Niiranen J, Balobanov V, Kiendl J, Hosseini SB (2019) Variational formulations, model comparisons and numerical methods for Euler–Bernoulli micro-and nano-beam models. Mathematics and Mechanics of Solids 24(1):312–335

Ogden RW (1997) Non-linear elastic deformations. Courier Corporation, Dover, Mineola

Pideri C, Seppecher P (1997) A second gradient material resulting from the homogenization of an heterogeneous linear elastic medium. Continuum Mechanics and Thermodynamics 9(5):241–257

Placidi L, dell'Isola F, Barchiesi E (2020) Heuristic homogenization of Euler and pantographic beams. In: Mechanics of Fibrous Materials and Applications, Springer, pp 123–155

Riks E (1972) The application of Newton's method to the problem of elastic stability. Journal of Applied Mechanics, Transactions ASME E(4):1060–1065

Rodrigues O (1840) Des lois géométriques qui régissent les déplacements d'un système solide dans l'espace, et de la variation des coordonnées provenant de ces déplacements considérés indépendamment des causes qui peuvent les produire. Journal de mathématiques pure at appliquées 1(5):380–440

Scerrato D, Giorgio I (2019) Equilibrium of two-dimensional cycloidal pantographic metamaterials in three-dimensional deformations. Symmetry 11(12):1523

Seppecher P, Alibert JJ, dell'Isola F (2011) Linear elastic trusses leading to continua with exotic mechanical interactions. In: Journal of Physics: Conference Series, IOP Publishing, vol 319, p 012018

Sheydakov DN, Altenbach H (2016) Stability of inhomogeneous micropolar cylindrical tube subject to combined loads. Mathematics and Mechanics of Solids 21(9):1082–1094

Solyaev Y, Lurie S, Barchiesi E, Placidi L (2020) On the dependence of standard and gradient elastic material constants on a field of defects. Mathematics and Mechanics of Solids 25(1):35–45

Spagnuolo M, Andreaus U (2019) A targeted review on large deformations of planar elastic beams: extensibility, distributed loads, buckling and post-buckling. Mathematics and Mechanics of Solids 24(1):258–280

Turco E (2018) Discrete is it enough? The revival of Piola–Hencky keynotes to analyze three-dimensional *Elastica*. Continuum Mechanics and Thermodynamics 30(5):1039–1057

Turco E, dell'Isola F, Cazzani A, Rizzi NL (2016) Hencky-type discrete model for pantographic structures: numerical comparison with second gradient continuum models. Zeitschrift für angewandte Mathematik und Physik 67(4):85

Turco E, Misra A, Sarikaya R, Lekszycki T (2019) Quantitative analysis of deformation mechanisms in pantographic substructures: experiments and modeling. Continuum Mechanics and Thermodynamics 31(1):209–223

Turco E, Barchiesi E, Giorgio I, dell'Isola F (2020) A Lagrangian Hencky-type non-linear model suitable for metamaterials design of shearable and extensible slender deformable bodies alternative to Timoshenko theory. International Journal of Non-Linear Mechanics 123:103481

Vangelatos Z, Komvopoulos K, Grigoropoulos C (2019a) Vacancies for controlling the behavior of microstructured three-dimensional mechanical metamaterials. Mathematics and Mechanics of Solids 24(2):511–524

Vangelatos Z, Melissinaki V, Farsari M, Komvopoulos K, Grigoropoulos C (2019b) Intertwined microlattices greatly enhance the performance of mechanical metamaterials. Mathematics and Mechanics of Solids 24(8):2636–2648

Wriggers P (2008) Nonlinear finite element methods. Springer Science & Business Media

Yang H, Ganzosch G, Giorgio I, Abali BE (2018) Material characterization and computations of a polymeric metamaterial with a pantographic substructure. Zeitschrift für angewandte Mathematik und Physik 69(4):105